Asthenosphere flow modulated by megathrust earthquake cycles

Sylvain Barbot[1]

[1]Earth Observatory of Singapore, Nanyang Technological University, Singapore

Key Points:

- Efficient earthquake cycles simulation at subduction zone combining boundary and volume elements in a curvilinear mesh.
- Large variations of effective viscosity during the seismic cycle result from nonlinear constitutive properties.
- Viscoelastic flow in the oceanic asthenosphere creates landward surface displacement in the postseismic period.

Corresponding author: Sylvain Barbot, `sbarbot@ntu.edu.sg`

Abstract

Subduction megathrusts develop the largest earthquakes, often close to large population centers. Understanding the dynamics of deformation at subduction zones is therefore important to better assess seismic hazards. Here, I develop consistent earthquake cycle simulations that incorporate localized and distributed deformation based on laboratory-derived constitutive laws by combining boundary and volume elements to represent the mechanical coupling between megathrust slip and solid-state flow in the oceanic asthenosphere and in the mantle wedge. The model is simplified, in two dimensions, but may help the interpretation of geodetic data. Megathrust earthquakes and slow-slip events modulate the strain-rate in the upper mantle, leading to large variations of effective viscosity in space and time and a complex pattern of surface deformation. While fault slip and flow in the mantle wedge generate surface displacements in the same, i.e., seaward, direction, the viscoelastic relaxation in the oceanic asthenosphere generates transient surface deformation in the opposite, i.e., landward, direction above the rupture area of the mainshock. Aseismic deformation above the seismogenic zone may be challenging to record, but it may reveal important constraints about the rheology of the subducting plate.

Introduction

The subduction of oceanic slabs beneath continents generates some of the largest earthquakes due to a wide, low-angle section cross-cutting the continental crust, where the frictional resistance is unstable [*Dieterich*, 1979; *Blanpied et al.*, 1995; *Nakatani*, 2001]. The largest historical earthquakes, the 1960 Mw 9.5 Valdivia, Chile [*Moreno et al.*, 2011], 1964 Mw 9.2 Alaska [*Plafker*, 1965], 2004 Mw 9.2 Sumatra [*Ishii et al.*, 2005; *Vigny et al.*, 2005], and the 2011 Mw 9.1 Tohoku, Japan [*Fujiwara et al.*, 2011] earthquakes all developed at subduction zones around the Rim of Fire and many remaining seismic gaps deserve close attention, notably the Nankai trough in Japan [*Hyodo and Hori*, 2013], the Mentawai islands in Sumatra [*Sieh et al.*, 2008; *Rubin et al.*, 2017; *Philibosian et al.*, 2017], the Guerrero section in Mexico [*Singh et al.*, 1981; *Astiz et al.*, 1987], the Cascadia in North America [*Heaton and Hartzell*, 1987; *Goldfinger et al.*, 2003], the Arakan in Myanmar [*Cummins*, 2007], the Makran in Iran [*Jackson and McKenzie*, 1984; *Heidarzadeh et al.*, 2008; *Heidarzadeh and Kijko*, 2011] and others elsewhere [*McCann et al.*, 1979; *Thatcher*, 1989; *Van Dissen and Berryman*, 1996].

Understanding the mechanics of earthquake production at subduction zones is key to better prepare for and mitigate seismic hazards. The magnitude of earthquakes is in part controlled by the rheology of the surrounding rocks, as megathrust earthquakes preferentially initiate and propagate in cold, strong rocks [*Scholz*, 2002; *Blanpied et al.*, 1995; *Scholz*, 1998]. A wide range of fault slip styles have now been identified down-dip megathrusts, including all of creep, slow-slip events, very-low frequency earthquakes, tsunami earthquakes, typical megathrust earthquakes, and giant ruptures [*Rogers and Dragert*, 2003; *Obara et al.*, 2004; *Wallace and Beavan*, 2006; *Ide*, 2012; *Radiguet et al.*, 2012; *Kato and Nakagawa*, 2014; *Plourde et al.*, 2015; *Suenaga et al.*, 2016; *Araki et al.*, 2017; *Nakamura*, 2017; *Nakano et al.*, 2018; *Toh et al.*, 2018; *Baba et al.*, 2018]. The style of rupture is dictated by the evolution of the frictional resistance during slip [*Collettini et al.*, 2011; *Leeman et al.*, 2016; *Mele Veedu and Barbot*, 2016; *Scuderi et al.*, 2017], the largest earthquakes probably involving strong weakening [*Toro et al.*, 2004; *Sone and Shimamoto*, 2009; *Noda and Lapusta*, 2013], but the rheology of country rocks may also play an important role [*Fagereng and Sibson*, 2010; *Noda and Shimamoto*, 2010; *Brantut et al.*, 2016; *Goswami and Barbot*, 2018].

Subduction is thought to be permitted by a low viscosity asthenosphere that allows the rigid tectonic plates to float on top relatively underformed [*Burke*, 2011]. However, the mechanical properties of the oceanic asthenosphere remain controversial, including the distribution of water, grain size, and the rheological characteristics of the lithosphere-asthenosphere boundary [*Mehouachi and Singh*, 2018]. The rheological structure of the mantle wedge is even more uncertain, as the region exhibits a complex pattern of metamorphism, dehydration, temperature, and small-scale convection [*Wada and Wang*, 2009]. Laboratory rock experiments constrain the rheological properties of olivine [*Mei and Kohlstedt*, 2000; *Karato and Jung*, 2003] and serpentinite [*Reinen et al.*, 1991; *Hilairet et al.*, 2007] well, but the in situ conditions remain elusive. As a result, there is no consensus on the effective viscosity at steady-state, the water content (and its spatial variations), and the pathways to arc volcanism [*Ohzono et al.*, 2012; *Hu et al.*, 2014; *Shibazaki et al.*, 2016; *Lee and Wada*, 2017] in the backarc.

Large earthquakes induce a significant stress change in the surrounding lithosphere [e.g., *Barbot et al.*, 2008; *Rousset et al.*, 2012; *Rollins et al.*, 2015; *Masuti et al.*, 2016; *Qiu et al.*, 2018, and references therein], leading to a transient acceleration of viscoelastic flow in the asthenosphere that is detectable in adequately designed geodetic networks [e.g., *Sathiakumar et al.*, 2017]. The postseismic deformation provides important constraints on distributed deformation at short time scales that in principle can provide additional insight into the constitutive properties and in situ conditions in the upper mantle [*Pollitz et al.*, 2006; *Wang et al.*, 2012; *Hu et al.*, 2014; *Broerse et al.*, 2015; *Bedford et al.*, 2016; *Masuti et al.*, 2016; *Klein et al.*, 2016; *Muto et al.*, 2016; *Govers et al.*, 2017; *Li et al.*, 2017, and references therein].

While there has been much progress in our understanding of rock mechanics from laboratory experiments [*Morrow et al.*, 2000; *Hirth and Kohlstedt*, 2003; *Han et al.*, 2007; *Ferri et al.*, 2010; *Brantut et al.*, 2011; *Hirth and Guillot*, 2013, and references therein], producing models of deformation that treat brittle and ductile behaviors consistently with realistic material properties still constitutes a challenge. This technical limitation hinders our understanding of the mechanics of the lithosphere-asthenosphere system across subduction zones. The deformation that accompanied and followed the 2011 Mw 9.2 Tohoku earthquake was captured across a wide frequency band by a large seismo-geodetic network [*Yagi and Fukahata*, 2011; *Nishimura et al.*, 2011; *Simons et al.*, 2011; *Wright et al.*, 2012; *Hooper et al.*, 2013], including offshore [*Iinuma et al.*, 2012, 2016; *Tomita et al.*, 2017]. The post-seismic deformation that followed the Tohoku earthquake seemed to contradict intuition. Seafloor geodesy data showed convincingly that the rupture area moved towards the ocean, as opposed to the expected landward direction for thrust-compatible motion. *Sun et al.* [2014] showed that this deformation was the hallmark of a low-viscosity oceanic asthenosphere responding to the coseismic stress perturbation. Recently, *Suito* [2017] and *Noda et al.* [2018] developed sophisticated models to decrypt the contributions of the asthenosphere and fault slip in surface observations following the Tohoku earthquake. These observations and modeling efforts demonstrate that more integrated models are needed to better understand and predict the deformation of the lithosphere.

Admittedly, subduction zones present some of the most challenging modeling settings in tectonophysics, including lateral variations of constitutive properties [*Hirahara*, 2002; *Wang*, 2007; *Muto*, 2011; *Muto et al.*, 2013, 2016] and important contributions from brittle and ductile deformation [*Freed et al.*, 2017]. The goal of this paper is to produce a simple reference model of a typical ocean-continent subduction zone to discuss the predictions of deformation throughout the seismic cycle based on reasonable assumptions about frictional and viscoelastic properties. This is accomplished using the integral method, combining boundary- and volume-elements to resolve all phases of the seismic cycle under rate-and-state friction - with the notable exception of the radiation of seismic waves - and the mechanical coupling between brittle and ductile deformation. The approach was introduced by *Lambert and Barbot* [2016] to model the seismic cycle in the lithosphere-asthenosphere system on long transform faults under the anti-plane strain approximation. It was extended to incorporating shear heating and heat diffusion by *Goswami and Barbot* [2018]. Here, I develop the method further to model the seismic cycle on long thrust faults in conditions of in-plane strain. The method used here should not be confused with finite-element modeling [e.g., *Malservisi et al.*, 2001; *Shibazaki et al.*, 2007; *Aagaard et al.*, 2013], where the governing equations are projected on basis functions and where the numerical solution is obtained by solving a large algebraic system. With the integral method, the solution is analytic, based on solving the governing equations exactly for a volume element, resulting in a more accurate and more numerically efficient solution. The numerical approximation lies in the spatial discretization of the fault and the surrounding volume. The displacement and stress kernels for a volume element can be used to directly image the anelastic deformation in Earth's interior [*Tsang et al.*, 2016; *Moore et al.*, 2017; *Qiu et al.*, 2018] and to simulate forward models of deformation [*Lambert and Barbot*, 2016; *Goswami and Barbot*, 2018]. The displacement and stress kernels for distributed deformation introduced by *Barbot et al.* [2017] are limited to a rectilinear geometry. To overcome this limitation, *Barbot* [2018] provided expressions for the displacement and stress kernels of triangle and tetrahedral elements, which is better suited for curvilinear meshing of topologically complex structures, such as subduction zones.

In the next section, I introduce the physical assumptions for modeling the seismic cycle and the viscoelastic flow in the upper mantle. Then, I describe the modeled dynamics of earthquakes and slow-slip events on the megathrust and how they modulate the effective viscosity in the upper mantle. I then describe the kinematics of surface deformation and the contributions of fault slip and viscoelastic flow throughout multiple earthquake cycles. The model reveals that viscoelastic flow in the oceanic asthenosphere creates transient landward displacements at the surface immediately above large earthquake ruptures. The large stress perturbation occasioned by earthquake ruptures induces a transient low-viscosity flow in the postseismic period followed by re-hardening.

Subduction dynamics with the integral method

The dynamics of the lithosphere during the seismic cycle is typically modeled with finite elements, a technique that allows realistic variations in elastic and viscoelastic properties and nonlinear constitutive laws. This approach has brought much insight into the rheology of plate boundaries at subduction zones [e.g., *Masterlark*, 2003; *Wang*, 2007; *Hu et al.*, 2014, 2016; *Klein et al.*, 2016; *Kyriakopoulos and Newman*, 2016], transform boundaries [e.g., *Masterlark and Wang*, 2002; *Freed and Bürgmann*, 2004; *Takeuchi and Fialko*, 2013; *Allison and Dunham*, 2017], and collision zones [*Cattin and Avouac*, 2000; *Liu et al.*, 2016; *Castaldo et al.*, 2017;

Wang and Fialko, 2018]. While finite-element modeling has proven versatile for forward and inverse modeling, notably using the adjoint method [*Crawford et al.*, 2016; *Agata et al.*, 2017], resolving the details of fault dynamics with this technique requires out-of-the-ordinary numerical resources and methods [*Agata et al.*, 2014; *Ichimura et al.*, 2016; *Uphoff et al.*, 2017]. Viscoelastic simulations have also exploited the correspondence principle, whereby heterogeneous effective elastic properties are mapped into the viscoelastic properties by virtue of the Fourier or Laplace transforms [*Pollitz*, 1992, 1997; *Smith and Sandwell*, 2004; *Fukahata and Matsu'ura*, 2006; *Chanard et al.*, 2018]. While elegant, this approach is limited to linear viscoelastic properties and often to vertical stratification of material properties, and ignores the coupling to brittle deformation, except for the work of *Kato* [2002]. Meanwhile, fault dynamics is efficiently simulated with the boundary-integral method [*Tse and Rice*, 1986; *Liu and Rice*, 2005; *Lapusta and Liu*, 2009; *Ando*, 2016], which is most efficient because only the fault surface is sampled numerically, the rest of the domain being accounted for analytically. It is natural to augment the boundary-integral method with volume elements to represent distributed deformation [*Lambert and Barbot*, 2016; *Barbot et al.*, 2017; *Goswami and Barbot*, 2018; *Barbot*, 2018]. This alternative approach, simply called the integral method, shares the advantages of the boundary-integral method but incorporates multi-physics, distributed deformation.

The subduction model consists in a trench-perpendicular cross-section of the half-space that includes the megathrust and the surrounding viscoelastic upper mantle (Figure 1). The fault is assumed planar, extends from the trench to 300 km towards the volcanic arc, from 0 to 30 km depth, and is discretized with $N = 200$ finite-width patches [*Okada*, 1992]. The oceanic asthenosphere is represented by an unstructured simplex mesh [*Persson and Strang*, 2004] of triangular elements [*Barbot*, 2018] confined in a polygon that mimics the shape of the subducting slab. The mantle wedge is represented by another set of triangular elements confined in a triangle region delimited by the continental crust (the upper boundary is close to the brittle-ductile transition), the down-going slab and an arbitrary lower limit of 300 km below which little viscoelastic deformation is expected. All triangles have sides of ~ 20 km, resulting in 907 triangular elements overall. The models with a finer mesh dimension of ~ 10 km show similar results, indicating numerical convergence for this specific setup.

The dynamics of fault slip is controlled by rate-and-state friction where the frictional resistance follows [*Dieterich*, 1979; *Ruina*, 1983]

$$\tau = \left[\mu_0 + a \ln \frac{V}{V_0} + b \ln \frac{\theta V_0}{L}\right] \bar{\sigma} \ , \tag{1}$$

with the aging law

$$\dot{\theta} = 1 - \frac{V\theta}{L} \ , \tag{2}$$

where a is the direct-effect parameter that controls the fracture energy and the velocity dependence of friction, b is another non-dimensional parameter that controls the degree of weakening and the dependence on the state variable, V_0 is a reference slip velocity, and L is a characteristic weakening distance that controls the critical nucleation size [*Ruina*, 1983; *Rubin and Ampuero*, 2005]

$$h^* = \frac{GL}{(b-a)\bar{\sigma}} \ . \tag{3}$$

Fault regions with the steady-state parameter $b-a < 0$ are stable, but fault regions of characteristic size R may generate spontaneous slip instabilities if $R > h^*$ [e.g., *Horowitz and Ruina*, 1989; *Lapusta and Barbot*, 2012]. For example, *Liu and Rice* [2005] showed that slow-slip events emerge spontaneously for $R/h^* \sim 1$ and *Mele Veedu and Barbot* [2016] established that period-doubling sequences of slow and fast ruptures occur for specific values of R/h^* close to unity. The fault is loaded with a background rate of $V_l = 10^{-9}$ m/s. The width of the seismogenic zone defined by the distribution of seismicity at subduction zones spans over a wide range but averages 96 ± 27 km [*Pacheco et al.*, 1993] or 112 ± 40 km [*Heuret et al.*, 2011], depending on the estimation technique used. For simplicity, I define the seismogenic zone on the megathrust by the region of the fault extending from 10 to 20 km that intersects the continental upper- and mid-crust. Because of the low dip angle of the megathrust, the resulting seismogenic zone is about 100 km wide, large enough to generate elasto-dynamic ruptures. While other models can explain long-term and short-term slow-slip events [e.g., *Matsuzawa et al.*, 2010; *Goswami and Barbot*, 2018], I follow *Liu and Rice* [2005] and model long-term slow-slip events as stable-weakening regions ($R/h^* \sim 1$) extending from 23 to 25 km depth (see Table 1).

In the upper mantle, the rheology of solid-state flow is dominated by the strength of olivine, the weakest and most abundant mineral. I assume that the viscoelastic flow is accommodated by a combination of diffusion creep and dislocation creep at steady-state, where the norm of the strain-rate follows

$$\begin{aligned} \dot{\epsilon} = {} & A_1 \left(C_{\mathrm{OH}}\right)^{r_1} \exp\left(-\frac{Q_1 + p\,\Omega_1}{RT}\right) \sigma^n \\ & + A_2 \left(C_{\mathrm{OH}}\right)^{r_2} d^{-m} \exp\left(-\frac{Q_2 + p\,\Omega_2}{RT}\right) \sigma \ , \end{aligned} \tag{4}$$

where $\dot{\epsilon}$ is the norm of the plastic strain-rate, C_{OH} is the water content, p is the overburden, T is the temperature, R is the universal gas constant, and σ is the norm of the deviatoric stress.

Dislocation creep is characterized by the activation energy Q_1 and activation volume Ω_1, the water sensitivity exponent r_1, the prefactor A_1, and the stress exponent $n = 3.5$. Diffusion creep is associated with the activation energy Q_2 and activation volume Ω_2, the water sensitivity exponent r_2, the grain size $d = 1$ mm, the grain size sensitivity exponent m, and the prefactor A_2. In the oceanic plate, the temperature follows the cooling half-space model with a plate age of $2{\times}10^{15}$ s, i.e., ~ 60 Myr and a basal mantle temperature of 1673 K. I use the constitutive properties of wet olivine with with 1,000 ppm H/Si reported by *Hirth and Kohlstedt* [2003] and summarized in Table 1. The seismic cycle overprints a longer time-scale tectonic deformation [*Herrendörfer et al.*, 2015; *Sobolev and Muldashev*, 2017] that can only be crudely approximated in short-term simulations. For the sake of simplicity, I assume that viscoelastic flow is driven by a background shortening rate of $\dot{\epsilon}^0_{22} = -10^{-15}$ /s.

In the mantle wedge, I assume that deformation is accommodated by diffusion creep and dislocation creep following (4) with the same constitutive parameters as in the oceanic mantle. However, I assume a large water content $C_{\text{OH}} = 10,000$ ppm H/Si in the mantle wedge corner up to 400 km away from the trench, associated with the dehydration of peridotite and arc volcanism, and a damped water content of $C_{\text{OH}} = 1,000$ ppm H/Si elsewhere (Figure 1). I also build a thermal profile assuming a slightly older plate age of ~ 70 Myr. This is obviously a simplification, but it reflects how the remaining uncertainties on the mantle wedge rheology still limit our understanding of this important region. For example, *Muto* [2011] and *Klein et al.* [2016] assume a lower viscosity at steady-state in the mantle wedge than in the oceanic mantle, but *Muto et al.* [2013] and *Muto et al.* [2016] consider the opposite. I also ignore the low-viscosity region below the volcanic arc [*Hu et al.*, 2014; *Muto et al.*, 2016] as it mainly affects the vertical displacement in the near field.

I simulate the evolution of traction, slip-rate and the state variable of the aging law on the megathrust and the three independent components of the stress tensor in the upper mantle using the integral method [*Lambert and Barbot*, 2016; *Goswami and Barbot*, 2018] over multiple earthquake cycles. I use the four/fifth-order accurate Runge Kutta method with adaptive time steps to model all stages of the seismic cycle within the radiation damping approximation. At each time step, I determine the slip acceleration using (1), the rate of the state variable using (2), and the strain-rate components $\dot{\epsilon}_{22}$, $\dot{\epsilon}_{23}$, and $\dot{\epsilon}_{33}$ following (4). To account for the full coupling of all the deformation processes, I convolve the rates of deformation with the traction and stress kernels and determine the resulting stress rates in the half-space. The rate of shear traction in the dip direction on the megathrust is obtained with

$$\dot{\tau} = K(V - V_l) + \sum_\beta M_\beta(\dot{\epsilon}_\beta - \dot{\epsilon}^0_\beta) - G\frac{\dot{V}}{2V_s} \ , \tag{5}$$

where K is the matrix of self interactions, the summation is over $\beta = 22, 23, 33$, and M_{22}, M_{23}, and M_{33} are the matrices of shear traction due to a unit strain in the volume elements for the components 22, 23, and 33, respectively. The term with the slip acceleration is the radiation damping. The rate of stress in the volume elements is given by

$$\dot{\sigma}_\alpha = J_\alpha(V - V_l) + \sum_\beta L_{\alpha\beta}\left(\dot{\epsilon}_\beta - \dot{\epsilon}^0_\beta\right) \ , \tag{6}$$

where α takes the values 22, 23, and 33, J_α is the stress caused by fault slip, which will cause postseismic relaxation, and $L_{\alpha\beta}$ are the matrices for stress change in the component α to due strain in the volume elements for the component β (see Supplementary Materials). The stress interactions matrices are calculated with analytic solutions [*Barbot*, 2018]. The simulation includes the nucleation, propagation, and arrest of large seismogenic-zone earthquakes and long-term slow-slip events, and the postseismic relaxation of the stress perturbation by afterslip on the megathrust and viscoelastic flow in the upper mantle. I simulate the deformation for 3,000 years, including 6 earthquakes, and about 120 slow-slip events. On my mid-2012, dual-core processor laptop with 8 Gb of memory, the calculation of the Green's function takes two minutes. The simulation requires about 50,000 time steps, which take 45 minutes to compute.

Dynamics of anelastic deformation at subduction zones

I describe the dynamics of fault slip and viscoelastic flow in the two-dimensional subduction zone model during the seismic cycle. With the combination of parameters discussed in the previous section, I obtain typical megathrust earthquakes that rupture the entire seismogenic zone every $\sim 500\,$yr. The long-term slow-slip events emerge every $\sim 25\,$yr, but their recurrence times are modulated by the earthquake cycle (Figures 2 and 3). Following each large rupture, afterslip propagates up-dip towards the trench and down-dip into the slow-slip region. The slow-slip events are accelerated for about $150\,$yr, after which they resume their natural recurrence pattern (Figure 3a). The accretionary prism undergoes creep, but this is a simplifying modeling assumption, as in reality this region undergoes a complex faulting style [*Hetland and Simons*, 2010; *Hubbard et al.*, 2015; *Suenaga et al.*, 2016; *Araki et al.*, 2017; *Nakano et al.*, 2018].

Each large earthquake induces a stress perturbation in the surrounding rocks that triggers a transient flow acceleration in the upper mantle. In the oceanic asthenosphere (dashed vertical profile in Figure 1), the postseismic relaxation takes 20 to 200 years, depending on the amplitude of the stress perturbation and the local effective viscosity (Figure 3b). After this, the flow continues at rates lower than steady state to preserve the long-term strain-rate. The accumulation of slow-slip events gradually accelerates viscoelastic flow in the oceanic asthenosphere, suggesting a possible mechanical coupling between the two mechanisms. During the postseismic transient the effective viscosity reduces from its background, steady-state value, by at least one order of magnitude, with a short excursion below $\eta_{\text{eff}} = 10^{19}\,\text{Pa s}$ (the lowest value being $2\times10^{18}\,\text{Pa s}$ in the oceanic mantle). This is compatible with several studies that require transient creep to explain the sudden drop of effective viscosity immediately after the earthquake [e.g., *Sun et al.*, 2014; *Klein et al.*, 2016; *Hu et al.*, 2016]. It is possible that nonlinear flow laws, not transient creep, are responsible for this effect. *Masuti et al.* [2016] found that a combination of both transient creep and nonlinear flow laws are required to explain the geodetic data following the 2012 Mw 8.6 Indian Ocean earthquake and *Qiu et al.* [2018] found that linear transient creep was the simplest way to explain the last decade of geodetic data along the Sumatran subduction zone (not excluding nonlinear transient creep). A more thorough comparison of the candidate rheological models is required to address the constitutive properties of the subducting slab.

The flow in the mantle wedge (dashed profile in Figure 1) is also modulated by the seismic cycle. With the rheological parameters chosen, the acceleration of viscoelastic flow is less pronounced than in the oceanic asthenosphere (Figure 3c,d). The strain rates are maximum between 450 and 600 km from the trench. The presence of a large water content in the mantle wedge corner does not lead to rapid flow there, presumably due to the dominant effect of low temperatures. It is possible that ductile or semi-brittle shear zones below the brittle-ductile transition afford faster relaxation transients [*Takeuchi and Fialko*, 2013; *Goswami and Barbot*, 2018]. More insight into the spatial distribution of serpentinized rocks and into the pathways of water and partial melt is needed to better constrain the rock rheology near the mantle wedge corner.

As recent studies demonstrate [*Sun et al.*, 2014; *Hu et al.*, 2016; *Suito*, 2017; *Noda et al.*, 2018], the surface deformation caused by the interaction of fault slip and mantle flow continues to surprise. In Figure 4, I describe the evolution of the trench-perpendicular surface displacement deficit, i.e, the difference between the displacement and the long-term average, throughout the seismic cycle. I establish the contributions of fault slip, flow in the oceanic asthenosphere, and flow in the mantle wedge to the surface displacements in space and time. This is done in a post-processing step by multiplying the slip or strain in the regions of interest by the respective Green's function for surface displacement. Above the megathrust, the displacement is dominated by fault slip, but its effect is reduced over time by the combined effect of slow-slip events and relocking. All of earthquakes, slow-slip events, afterslip, and creep create seaward displacement. Postseismic relaxation in the oceanic asthenosphere is the only mechanism that creates significant landward displacements above the megathrust during the postseismic period. These accumulate within a few years following large earthquakes and largely recede late in the seismic cycle. The flow in the oceanic asthenosphere also creates landward displacements in the outer rise and on land (i.e., more than 300 km from the trench). With the modeling assumptions presented in the previous section, the viscoelastic flow in the mantle wedge creates a lower-amplitude postseismic relaxation than flow in the oceanic lithosphere by a factor of 7, but it still contributes significantly to the surface displacements on land. There, all sources of deformation produce displacements in the same direction. The amplitude of these different contributions would be largely affected by, among others, the size of the earthquakes, the age of the subducting plates, and the rheology of the mantle wedge.

While the patterns of the model are not expected to change significantly within modest variations from the modeling assumptions, some adjustments may be needed to fit particular tectonic contexts and explain local geophysical data. The seismic cycle at subduction zones is certainly more complex than that illustrated in the current model. Long seismic cycles that exhibit partial and full ruptures of the megathrust or a wider range of earthquake sizes and slip speeds can occur in models with a higher ratio of the seismogenic zone to the nucleation size [*Horowitz and Ruina*, 1989; *Rice*, 1993; *Nielsen et al.*, 2000; *Kato*, 2003; *Wu and Chen*, 2014; *Michel et al.*, 2017], with morphological gradients [*Qiu et al.*, 2016; *Biemiller and Lavier*, 2017; *Romanet et al.*, 2018], or strong-weakening mechanisms. Along-strike variations in frictional and off-fault properties may also introduce additional complexity [e.g., *Yabe and Ide*, 2017].

Conclusions

I describe how the integral method can be used to simulate the seismic cycle at subduction zones to couple fault slip and viscoelastic strain. The approach is computationally efficient, and may resolve all the phases of the seismic cycle including off-fault deformation, but excluding the radiation of seismic waves. The model integrates laboratory-derived constitutive laws for friction and plastic flow. While more data are needed to constrain the rheology of the mantle wedge in particular, the model may constitute a reference point to understand the dynamics of subduction zones, i.e., predict quasi-static deformation, prepare seismo-geodetic networks, and test the merit of alternate models.

The postseismic relaxation in the oceanic asthenosphere that follows large earthquakes is characterized by a transient flow with a low effective viscosity explained by the nonlinear stress dependence of dislocation creep. Flow in the oceanic asthenosphere creates landward surface displacements above the coseismic rupture and seaward displacements away from it. Offshore geodetic data are admittedly challenging to obtain, despite recent progress [*Wallace et al.*, 2016; *Yokota et al.*, 2016; *Maksymowicz et al.*, 2017; *Tomita et al.*, 2017], but these measurements may be most effective to constrain the rheology of the subducting slab and fault processes near the trench. The rheological properties of the mantle wedge are less well constrained, but viscoelastic flow in the backarc contributes significantly to postseismic deformation, producing displacement compatible with all other deformation mechanisms above the land.

While the modeling technique introduced here is still in its infancy, it represent a potentially efficient approach to model deformation in tectonically complex settings. Further applications of the integral method to three-dimensional problems may bring new insight into the mechanics of subduction zones.

Acknowledgments

The software used in this study is hosted at https://bitbucket.org/sbarbot/unicycle. This research was supported by the National Research Foundation of Singapore under the NRF Fellowship scheme (National Research Fellow Awards No. NRF-NRFF2013-04) and by the Earth Observatory of Singapore, the National Research Foundation, and the Singapore Ministry of Education under the Research Centres of Excellence initiative. This work comprises Earth Observatory of Singapore contribution no. 191.

References

Aagaard, B. T., M. G. Knepley, and C. A. Williams (2013), A domain decomposition approach to implementing fault slip in finite-element models of quasi-static and dynamic crustal deformation, *J. Geophys. Res.*, *118*(6), 3059–3079.

Agata, R., T. Ichimura, K. Hirahara, M. Hyodo, T. Hori, and M. Hori (2014), Several hundred finite element analyses of an inversion of earthquake fault slip distribution using a high-fidelity model of the crustal structure, *Procedia Computer Science*, *29*, 877–887.

Agata, R., T. Ichimura, T. Hori, K. Hirahara, C. Hashimoto, and M. Hori (2017), An adjoint-based simultaneous estimation method of the asthenosphere's viscosity and afterslip using a fast and scalable finite element adjoint solver, *Geophysical Journal International*.

Allison, K. L., and E. M. Dunham (2017), Earthquake cycle simulations with rate-and-state friction and power-law viscoelasticity, *Tectonophysics*.

Ando, R. (2016), On applications of fast domain partitioning method to earthquake simulations with spatiotemporal boundary integral equation method, in *International Conference Continuum Mechanics Focusing on Singularities*, pp. 87–99, Springer.

Araki, E., D. M. Saffer, A. J. Kopf, L. M. Wallace, T. Kimura, Y. Machida, S. Ide, E. Davis, I. Expedition, et al. (2017), Recurring and triggered slow-slip events near the trench at the nankai trough subduction megathrust, *Science*, *356*(6343), 1157–1160.

Astiz, L., H. Kanamori, and H. Eissler (1987), Source characteristics of earthquakes in the michoacan seismic gap in mexico, *Bull. Seism. Soc. Am.*, *77*(4), 1326–1346.

Baba, S., A. Takeo, K. Obara, A. Kato, T. Maeda, and T. Matsuzawa (2018), Temporal activity modulation of deep very low frequency earthquakes in shikoku, southwest japan, *Geophys. Res. Lett.*

Barbot, S. (2018), Displacement and stress induced by anelastic deformation confined in a tetrahedral volume, *Bull. Seism. Soc. Am.*, doi:arXiv:1802.06313.

Barbot, S., Y. Hamiel, and Y. Fialko (2008), Space geodetic investigation of the coseismic and postseismic deformation due to the 2003 Mw 7.2 Altai earthquake: Implications for the local lithospheric rheology, *J. Geophys. Res.*, *113*(B03403), doi: 10.1029/2007JB005063.

Barbot, S., J. D. Moore, and V. Lambert (2017), Displacement and stress associated with distributed anelastic deformation in a half-space, *Bull. Seism. Soc. Am.*, *107*(2), 821–855.

Bedford, J., M. Moreno, S. Li, O. Oncken, J. C. Baez, M. Bevis, O. Heidbach, and D. Lange (2016), Separating rapid relocking, afterslip, and viscoelastic relaxation: An application of the postseismic straightening method to the maule 2010 cgps, *Journal of Geophysical Research: Solid Earth*, *121*(10), 7618–7638.

Biemiller, J., and L. Lavier (2017), Earthquake supercycles as part of a spectrum of normal fault slip styles, *Journal of Geophysical Research: Solid Earth*, *122*(4), 3221–3240.

Blanpied, M. L., D. A. Lockner, and J. D. Byerlee (1995), Frictional slip of granite at hydrothermal conditions, *J. Geophys. Res.*, *100*(B7), 13,045–13,064.

Brantut, N., J. Sulem, and A. Schubnel (2011), Effect of dehydration reactions on earthquake nucleation: Stable sliding, slow transients, and unstable slip, *J. Geophys. Res.*, *116*(B5).

Brantut, N., F. X. Passelègue, D. Deldicque, J.-N. Rouzaud, and A. Schubnel (2016), Dynamic weakening and amorphization in serpentinite during laboratory earthquakes, *Geology*, *44*(8), 607–610.

Broerse, T., R. Riva, W. Simons, R. Govers, and B. Vermeersen (2015), Postseismic grace and gps observations indicate a rheology contrast above and below the sumatra slab, *Journal of Geophysical Research: Solid Earth*, *120*(7), 5343–5361.

Burke, K. (2011), Plate tectonics, the wilson cycle, and mantle plumes: geodynamics from the top, *Annual Review of Earth and Planetary Sciences*, *39*, 1–29.

Castaldo, R., V. De Novellis, G. Solaro, S. Pepe, P. Tizzani, C. De Luca, M. Bonano, M. Manunta, F. Casu, I. Zinno, et al. (2017), Finite element modelling of the 2015 gorkha earthquake through the joint exploitation of dinsar measurements and geologic-structural information, *Tectonophysics*, *714*, 125–132.

Cattin, R., and J. P. Avouac (2000), Modeling mountain building and the seismic cycle in the Himalaya of Nepal, *J. Geophys. Res.*, *105*(B6), 13,389–13,407.

Chanard, K., L. Fleitout, E. Calais, S. Barbot, and J.-P. Avouac (2018), Constraints on transient viscoelastic rheology of the asthenosphere from seasonal deformation, *Geophysical Research Letters*, *45*(5), 2328–2338.

Collettini, C., A. Niemeijer, C. Viti, S. A. Smith, and C. Marone (2011), Fault structure, frictional properties and mixed-mode fault slip behavior, *Earth Planet. Sci. Lett.*, *311*(3), 316–327.

Crawford, O., D. Al-Attar, J. Tromp, and J. X. Mitrovica (2016), Forward and inverse modelling of post-seismic deformation, *Geophysical journal international*, p. ggw414.

Cummins, P. R. (2007), The potential for giant tsunamigenic earthquakes in the northern bay of bengal, *Nature*, *449*(7158), 75.

Dieterich, J. H. (1979), Modeling of rock friction 1. experimental results and constitutive equations, *J. Geophys. Res.*, *84*(B5), 2161–2168.

Fagereng, Å., and R. H. Sibson (2010), Melange rheology and seismic style, *Geology*, *38*(8), 751–754.

Ferri, F., G. D. Toro, T. Hirose, and T. Shimamoto (2010), Evidence of thermal pressurization in high-velocity friction experiments on smectite-rich gouges, *Terra Nova*, *22*(5), 347–353.

Freed, A. M., and R. Bürgmann (2004), Evidence of power-law flow in the Mojave desert mantle, *Nature*, *430*, 548–551.

Freed, A. M., A. Hashima, T. W. Becker, D. A. Okaya, H. Sato, and Y. Hatanaka (2017), Resolving depth-dependent subduction zone viscosity and afterslip from postseismic displacements following the 2011 tohoku-oki, japan earthquake, *Earth and Planetary Science Letters*, *459*, 279–290.

Fujiwara, T., S. Kodaira, T. No, Y. Kaiho, N. Takahashi, and Y. Kaneda (2011), The 2011 tohoku-oki earthquake: Displacement reaching the trench axis, *Science*, *334*(6060), 1240–1240.

Fukahata, Y., and M. Matsu'ura (2006), Quasi-static internal deformation due to a dislocation source in a multilayered elastic/viscoelastic half-space and an equivalence theorem, *Geophysical Journal International*, *166*(1), 418–434.

Goldfinger, C., C. Hans Nelson, J. E. Johnson, et al. (2003), Deep-water turbidites as holocene earthquake proxies: the cascadia subduction zone and northern san andreas fault systems, *Annals of Geophysics*.

Goswami, A., and S. Barbot (2018), Slow-slip events in semi-brittle serpentinite fault zones, *Scientific reports*, *8*(1), 6181.

Govers, R., K. Furlong, L. Wiel, M. Herman, and T. Broerse (2017), The geodetic signature of the earthquake cycle at subduction zones: Model constraints on the deep processes, *Reviews of Geophysics*.

Han, R., T. Shimamoto, T. Hirose, J.-H. Ree, and J. Ando (2007), Ultralow friction of carbonate faults caused by thermal decomposition, *Science*, *316*, doi: 10.1126/science.1139763.

Heaton, T. H., and S. H. Hartzell (1987), Earthquake hazards on the cascadia subduction zone, *Science*, *236*(4798), 162–168.

Heidarzadeh, M., and A. Kijko (2011), A probabilistic tsunami hazard assessment for the makran subduction zone at the northwestern indian ocean, *Natural hazards*, *56*(3), 577–593.

Heidarzadeh, M., M. D. Pirooz, N. H. Zaker, A. C. Yalciner, M. Mokhtari, and A. Esmaeily (2008), Historical tsunami in the makran subduction zone off the southern coasts of iran and pakistan and results of numerical modeling, *Ocean Engineering*, *35*(8-9), 774–786.

Herrendörfer, R., Y. Van Dinther, T. Gerya, and L. A. Dalguer (2015), Earthquake supercycle in subduction zones controlled by the width of the seismogenic zone, *Nature Geoscience*, *8*(6), 471–474.

Hetland, E., and M. Simons (2010), Post-seismic and interseismic fault creep ii: transient creep and interseismic stress shadows on megathrusts, *Geophysical Journal International*, *181*(1), 99–112.

Heuret, A., S. Lallemand, F. Funiciello, C. Piromallo, and C. Faccenna (2011), Physical characteristics of subduction interface type seismogenic zones revisited, *Geochemistry, Geophysics, Geosystems*, *12*(1).

Hilairet, N., B. Reynard, Y. Wang, I. Daniel, S. Merkel, N. Nishiyama, and S. Petitgirard (2007), High-pressure creep of serpentine, interseismic deformation, and initiation of subduction, *Science*, *318*(5858), 1910–1913.

Hirahara, K. (2002), Interplate earthquake fault slip during periodic earthquake cycles in a viscoelastic medium at a subduction zone, *Pure and applied geophysics*, *159*(10), 2201–2220.

Hirth, G., and S. Guillot (2013), Rheology and tectonic significance of serpentinite, *Elements*, *9*(2), 107–113.

Hirth, G., and D. L. Kohlstedt (2003), Rheology of the upper mantle and the mantle wedge: a view from the experimentalists, in *Inside the Subduction Factory*, *Geophys. Monogr.*, vol. 138, edited by J. Eiler, pp. 83–105, Am. Geophys. Soc., Washington, D. C.

Hooper, A., J. Pietrzak, W. Simons, H. Cui, R. Riva, M. Naeije, A. T. van Scheltinga, E. Schrama, G. Stelling, and A. Socquet (2013), Importance of horizontal seafloor motion on tsunami height for the 2011 mw= 9.0 tohoku-oki earthquake, *Earth and Planetary Science Letters*, *361*, 469–479.

Horowitz, F. G., and A. Ruina (1989), Slip patterns in a spatially homogeneous fault model, *J. Geophys. Res.*, *94*(B8), 10,279–10,298.

Hu, Y., R. Bürgmann, J. T. Freymueller, P. Banerjee, and K. Wang (2014), Contributions of poroelastic rebound and a weak volcanic arc to the postseismic deformation of the 2011 tohoku earthquake, *Earth, Planets and Space*, *66*(1), 106.

Hu, Y., R. Bürgmann, N. Uchida, P. Banerjee, and J. T. Freymueller (2016), Stress-driven relaxation of heterogeneous upper mantle and time-dependent afterslip following the 2011 tohoku earthquake, *Journal of Geophysical Research: Solid Earth*, *121*(1), 385–411.

Hubbard, J., S. Barbot, E. M. Hill, and P. Tapponnier (2015), Coseismic slip on shallow décollement megathrusts: implications for seismic and tsunami hazard, *Earth-Science Reviews*, *141*, 45–55.

Hyodo, M., and T. Hori (2013), Re-examination of possible great interplate earthquake scenarios in the nankai trough, southwest japan, based on recent findings and numerical simulations, *Tectonophysics*, *600*, 175–186.

Ichimura, T., R. Agata, T. Hori, K. Hirahara, C. Hashimoto, M. Hori, and Y. Fukahata (2016), An elastic/viscoelastic finite element analysis method for crustal deformation using a 3-d island-scale high-fidelity model, *Geophysical Journal International*, *206*(1), 114–129.

Ide, S. (2012), Variety and spatial heterogeneity of tectonic tremor worldwide, *J. Geophys. Res.*, *117*(B3).

Iinuma, T., R. Hino, M. Kido, D. Inazu, Y. Osada, Y. Ito, M. Ohzono, H. Tsushima, S. Suzuki, H. Fujimoto, et al. (2012), Coseismic slip distribution of the 2011 off the pacific coast of tohoku earthquake (m9. 0) refined by means of seafloor geodetic data, *Journal of Geophysical Research: Solid Earth*, *117*(B7).

Iinuma, T., R. Hino, N. Uchida, W. Nakamura, M. Kido, Y. Osada, and S. Miura (2016), Seafloor observations indicate spatial separation of coseismic and postseismic slips in the 2011 tohoku earthquake, *Nature communications*, *7*, 13,506.

Ishii, M., P. M. Shearer, H. Houston, and J. E. Vidale (2005), Extent, duration and speed of the 2004 sumatra–andaman earthquake imaged by the hi-net array, *Nature*, *435*(7044), 933.

Jackson, J., and D. McKenzie (1984), Active tectonics of the alpine–himalayan belt between western turkey and pakistan, *Geophysical Journal International*, *77*(1), 185–264.

Karato, S.-I., and H. Jung (2003), Effects of pressure on high-temperature dislocation creep in olivine, *Philosophical Magazine*, *83*(3), 401–414.

Kato, A., and S. Nakagawa (2014), Multiple slow-slip events during a foreshock sequence of the 2014 iquique, chile mw 8.1 earthquake, *Geophys. Res. Lett.*, *41*(15), 5420–5427.

Kato, N. (2002), Seismic cycle on a strike-slip fault with rate-and state-dependent strength in an elastic layer overlying a viscoelastic half-space, *Earth, planets and space*, *54*(11), 1077–1083.

Kato, N. (2003), Repeating slip events at a circular asperity: Numerical simulation with a rate-and state-dependent friction law, *Bull. Earthq. Res. Inst. Univ. Tokyo*, *78*, 151–166.

Klein, E., L. Fleitout, C. Vigny, and J. Garaud (2016), Afterslip and viscoelastic relaxation model inferred from the large-scale post-seismic deformation following the 2010 m w 8.8 maule earthquake (chile), *Geophysical Journal International*, *205*(3), 1455–1472.

Kyriakopoulos, C., and A. Newman (2016), Structural asperity focusing locking and earthquake slip along the nicoya megathrust, costa rica, *Journal of Geophysical Research: Solid Earth*, *121*(7), 5461–5476.

Lambert, V., and S. Barbot (2016), Contribution of viscoelastic flow in earthquake cycles within the lithosphere-asthenosphere system, *Geophys. Res. Lett.*, *43*(19), 142–154.

Lapusta, N., and S. Barbot (2012), Models of earthquakes and aseismic slip based on laboratory-derived rate and state friction laws, in *The mechanics of Faulting: From Laboratory to Real Earthquakes*, edited by A. Bizzarri and H. S. Bhat, pp. 153–207, Research Signpost, Trivandrum, Kerala, India.

Lapusta, N., and Y. Liu (2009), Three-dimensional boundary integral modeling of spontaneous earthquake sequences and aseismic slip, *J. Geophys. Res.*, *114*(B09303), 25 PP.

Lee, C., and I. Wada (2017), Clustering of arc volcanoes caused by temperature perturbations in the back-arc mantle, *Nature Communications*, *8*, 15,753.

Leeman, J., D. Saffer, M. Scuderi, and C. Marone (2016), Laboratory observations of slow earthquakes and the spectrum of tectonic fault slip modes, *Nature communications*, *7*, 11,104.

Li, S., M. Moreno, J. Bedford, M. Rosenau, O. Heidbach, D. Melnick, and O. Oncken (2017), Postseismic uplift of the andes following the 2010 maule earthquake: Implications for mantle rheology, *Geophysical Research Letters*, *44*(4), 1768–1776.

Liu, C., B. Zhu, X. Yang, and Y. Shi (2016), Geodynamic background of the 2008 wenchuan earthquake based on 3d visco-elastic numerical modelling, *Physics of the Earth and Planetary Interiors*, *252*, 23–36.

Liu, Y., and J. R. Rice (2005), Aseismic slip transients emerge spontaneously in three-dimensional rate and state modeling of subduction earthquake sequences, *J. Geophys.*

Res., *110*(B08307), doi:10.1029/2004JB003424.

Maksymowicz, A., C. Chadwell, J. Ruiz, A. Tréhu, E. Contreras-Reyes, W. Weinrebe, J. Díaz-Naveas, J. Gibson, P. Lonsdale, and M. Tryon (2017), Coseismic seafloor deformation in the trench region during the mw8. 8 maule megathrust earthquake, *Scientific reports*, *7*, 45,918.

Malservisi, R., K. Furlong, and T. H. Dixon (2001), Influence of the earthquake cycle and lithospheric rheology on the dynamics of the eastern california shear zone, *Geophysical Research Letters*, *28*(14), 2731–2734.

Masterlark, T. (2003), Finite element model predictions of static deformation from dislocation sources in a subduction zone: sensitivities to homogeneous, isotropic, poisson-solid, and half-space assumptions, *Journal of Geophysical Research: Solid Earth*, *108*(B11).

Masterlark, T., and H. F. Wang (2002), Transient Stress-Coupling Between the 1992 Landers and 1999 Hector Mine, California, Earthquakes, *Bull. Seism. Soc. Am.*, *92*(4), 1470–1486, doi:10.1785/0120000905.

Masuti, S., S. Barbot, S. Karato, L. Feng, and P. Banerjee (2016), Upper mantle water stratification inferred from the 2012 Mw 8.6 Indian Ocean earthquake, *Nature*, *538*, 373–377.

Matsuzawa, T., H. Hirose, B. Shibazaki, and K. Obara (2010), Modeling short- and long-term slow slip events in the seismic cycles of large subduction earthquakes, *J. Geophys. Res.*, *115*(B12301), doi:10.1029/2010JB007566.

McCann, W., S. Nishenko, L. Sykes, and J. Krause (1979), Seismic gaps and plate tectonics: seismic potential for major boundaries, in *Earthquake Prediction and Seismicity Patterns*, pp. 1082–1147, Springer.

Mehouachi, F., and S. C. Singh (2018), Water-rich sublithospheric melt channel in the equatorial atlantic ocean, *Nature Geoscience*, *11*(1), 65.

Mei, S., and D. Kohlstedt (2000), Influence of water on plastic deformation of olivine aggregates: 1. diffusion creep regime, *Journal of Geophysical Research: Solid Earth*, *105*(B9), 21,457–21,469.

Mele Veedu, M., and S. Barbot (2016), The Parkfield tremors reveal slow and fast ruptures on the same asperity, *Nature*, *532*(7599), 361–365.

Michel, S., J.-P. Avouac, N. Lapusta, and J. Jiang (2017), Pulse-like partial ruptures and high-frequency radiation at creeping-locked transition during megathrust earthquakes, *Geophys. Res. Lett.*, *44*(16), 8345–8351.

Moore, J. D., H. Yu, C.-H. Tang, T. Wang, S. Barbot, D. Peng, S. Masuti, J. Dauwels, Y.-J. Hsu, V. Lambert, et al. (2017), Imaging the distribution of transient viscosity after the 2016 mw 7.1 kumamoto earthquake, *Science*, *356*(6334), 163–167.

Moreno, M., D. Melnick, M. Rosenau, J. Bolte, J. Klotz, H. Echtler, J. Baez, K. Bataille, J. Chen, M. Bevis, et al. (2011), Heterogeneous plate locking in the south–central chile subduction zone: Building up the next great earthquake, *Earth and Planetary Science Letters*, *305*(3-4), 413–424.

Morrow, C., D. E. Moore, and D. Lockner (2000), The effect of mineral bond strength and adsorbed water on fault gouge frictional strength, *Geophys. Res. Lett.*, *27*(6), 815–818.

Muto, J. (2011), Rheological structure of northeastern japan lithosphere based on geophysical observations and rock mechanics, *Tectonophysics*, *503*(3-4), 201–206.

Muto, J., B. Shibazaki, Y. Ito, T. Iinuma, M. Ohzono, T. Matsumoto, and T. Okada (2013), Two-dimensional viscosity structure of the northeastern japan islands arc-trench system, *Geophys. Res. Lett.*, *40*(17), 4604–4608.

Muto, J., B. Shibazaki, T. Iinuma, Y. Ito, Y. Ohta, S. Miura, and Y. Nakai (2016), Heterogeneous rheology controlled postseismic deformation of the 2011 tohoku-oki earthquake, *Geophys. Res. Lett.*, *43*(10), 4971–4978.

Nakamura, M. (2017), Distribution of low-frequency earthquakes accompanying the very low frequency earthquakes along the ryukyu trench, *Earth, Planets and Space*, *69*(1), 49.

Nakano, M., T. Hori, E. Araki, S. Kodaira, and S. Ide (2018), Shallow very-low-frequency earthquakes accompany slow slip events in the nankai subduction zone, *Nature communications*, *9*(1), 984.

Nakatani, M. (2001), Conceptual and physical clarification of rate and state friction: Frictional sliding as a thermally activated rheology, *J. Geophys. Res.*, *106*(B7), 13,347–13,380.

Nielsen, S. B., J. Carlson, and K. B. Olsen (2000), Influence of friction and fault geometry on earthquake rupture, *J. Geophys. Res.*, *105*(B3), 6069–6088.

Nishimura, T., H. Munekane, and H. Yarai (2011), The 2011 off the pacific coast of tohoku earthquake and its aftershocks observed by geonet, *Earth, planets and space*, *63*(7), 22.

Noda, A., T. Takahama, T. Kawasato, and M. Matsu?ura (2018), Interpretation of offshore crustal movements following the 2011 tohoku-oki earthquake by the combined effect of afterslip and viscoelastic stress relaxation, *Pure and Applied Geophysics*, *175*(2), 559–572.

Noda, H., and N. Lapusta (2013), Stable creeping fault segments can become destructive as a result of dynamic weakening, *Nature*, *493*(7433), 518–521.

Noda, H., and T. Shimamoto (2010), A rate- and state-dependent ductile flow law of polycrystalline halite under large shear strain and implications for transition to brittle deformation, *Geophys. Res. Lett.*, *37*(L09310), doi:10.1029/2010GL042512.

Obara, K., H. Hirose, F. Yamamizu, and K. Kasahara (2004), Episodic slow slip events accompanied by non-volcanic tremors in southwest japan subduction zone, *Geophys. Res. Lett.*, *31*(23).

Ohzono, M., Y. Ohta, T. Iinuma, S. Miura, and J. Muto (2012), Geodetic evidence of viscoelastic relaxation after the 2008 iwate-miyagi nairiku earthquake, *Earth, planets and space*, *64*(9), 759–764.

Okada, Y. (1992), Internal deformation due to shear and tensile faults in a half-space, *Bull. Seism. Soc. Am.*, *82*, 1018–1040.

Pacheco, J. F., L. R. Sykes, and C. H. Scholz (1993), Nature of seismic coupling along simple plate boundaries of the subduction type, *J. Geophys. Res.*, *98*(B8), 14,133–14,159.

Persson, P.-O., and G. Strang (2004), A simple mesh generator in matlab, *SIAM review*, *46*(2), 329–345.

Philibosian, B., K. Sieh, J.-P. Avouac, D. H. Natawidjaja, H.-W. Chiang, C.-C. Wu, C.-C. Shen, M. R. Daryono, H. Perfettini, B. W. Suwargadi, et al. (2017), Earthquake supercycles on the mentawai segment of the sunda megathrust in the seventeenth century and earlier, *Journal of Geophysical Research: Solid Earth*, *122*(1), 642–676.

Plafker, G. (1965), Tectonic deformation associated with the 1964 alaska earthquake: The earthquake of 27 march 1964 resulted in observable crustal deformation of unprecedented areal extent, *Science*, *148*(3678), 1675–1687.

Plourde, A. P., M. G. Bostock, P. Audet, and A. M. Thomas (2015), Low-frequency earthquakes at the southern cascadia margin, *Geophys. Res. Lett.*, *42*(12), 4849–4855.

Pollitz, F. F. (1992), Postseismic relaxation theory on the spherical earth, *Bulletin of the Seismological Society of America*, *82*(1), 422–453.

Pollitz, F. F. (1997), Gravitational viscoelastic postseismic relaxation on a layered spherical Earth, *J. Geophys. Res.*, *102*, 17,921–17,941.

Pollitz, F. F., R. Bürgmann, and P. Banerjee (2006), Post-seismic relaxation following the great 2004 Sumatra-Andaman earthquake on a compressible self-gravitating Earth, *Geophys. J. Int.*, *167*(1), 397–420.

Qiu, Q., E. M. Hill, S. Barbot, J. Hubbard, W. Feng, E. O. Lindsey, L. Feng, K. Dai, S. V. Samsonov, and P. Tapponnier (2016), The mechanism of partial rupture of a locked megathrust: The role of fault morphology, *Geology*, *44*(10), 875–878.

Qiu, Q., J. D. P. Moore, S. Barbot, L. Feng, and E. Hill (2018), Transient viscosity in the Sumatran mantle wedge from a decade of geodetic observations, *Nature Communications*.

Radiguet, M., F. Cotton, M. Vergnolle, M. Campillo, A. Walpersdorf, N. Cotte, and V. Kostoglodov (2012), Slow slip events and strain accumulation in the guerrero gap, mexico, *J. Geophys. Res.*, *117*(B4).

Reinen, L. A., J. D. Weeks, and T. E. Tullis (1991), The frictional behavior of serpentinite: Implications for aseismic creep on shallow crustal faults, *Geophys. Res. Lett.*, *18*(10), 1921–1924, doi:10.1029/91GL02367.

Rice, J. R. (1993), Spatio-temporal complexity of slip on a fault, *J. Geophys. Res.*, *98*(B6), 9885–9907.

Rogers, G., and H. Dragert (2003), Episodic tremor and slip on the Cascadia subduction zone: The chatter of silent slip, *Science*, *300*(5627), doi:10.1126/science.1084783.

Rollins, J. C., S. Barbot, and J.-P. Avouac (2015), Mechanisms of postseismic deformation following the 2010 el mayor-cucapah earthquake, *Pure App. Geophys.*, p. 54.

Romanet, P., H. S. Bhat, R. Jolivet, and R. Madariaga (2018), Fast and slow slip events emerge due to fault geometrical complexity, *Geophys. Res. Lett.*

Rousset, B., S. Barbot, J. P. Avouac, and Y.-J. Hsu (2012), Postseismic Deformation Following the 1999 Chi-Chi Earthquake, Taiwan: Implication for Lower-Crust Rheology, *J. Geophys. Res.*, *117*(B12405), 16.

Rubin, A. M., and J.-P. Ampuero (2005), Earthquake nucleation on (aging) rate and state faults, *J. Geophys. Res.*, *110*(B11312), 24 PP.

Rubin, C. M., B. P. Horton, K. Sieh, J. E. Pilarczyk, P. Daly, N. Ismail, and A. C. Parnell (2017), Highly variable recurrence of tsunamis in the 7,400 years before the 2004 indian ocean tsunami, *Nature communications*, *8*, 16,019.

Ruina, A. (1983), Slip instability and state variable friction laws, *J. Geophys. Res.*, *88*, 10,359–10,370.

Sathiakumar, S., S. Barbot, and P. Agram (2017), Extending resolution of fault slip with geodetic data through optimal network design, *J. Geophys. Res.*

Scholz, C. H. (1998), Earthquakes and friction laws, *Nature*, *391*, 37–42.

Scholz, C. H. (2002), *The mechanics of earthquakes and faulting*, 2nd Ed., 496 pp., Cambidge Univ. Press, New York, NY.

Scuderi, M. M., C. Collettini, C. Viti, E. Tinti, and C. Marone (2017), Evolution of shear fabric in granular fault gouge from stable sliding to stick slip and implications for fault slip mode, *Geology*, *45*(8), 731–734.

Shibazaki, B., K. Garatani, and H. Okuda (2007), Finite element analysis of crustal deformation in the ou backbone range, northeastern japan, with non-linear visco-elasticity and plasticity: effects of non-uniform thermal structure, *Earth, Planets and Space*, *59*(6), 499–512.

Shibazaki, B., T. Okada, J. Muto, T. Matsumoto, T. Yoshida, and K. Yoshida (2016), Heterogeneous stress state of island arc crust in northeastern japan affected by hot mantle fingers, *Journal of Geophysical Research: Solid Earth*, *121*(4), 3099–3117.

Sieh, K., D. H. Natawidjaja, A. J. Meltzner, C.-C. Shen, H. Cheng, K.-S. Li, B. W. Suwargadi, J. Galetzka, B. Philibosian, and R. L. Edwards (2008), Earthquake supercycles inferred from sea-level changes recorded in the corals of West Sumatra, *Science*, *322*, 1674–1678.

Simons, M., S. E. Minson, A. Sladen, F. Ortega, J. Jiang, S. E. Owen, L. Meng, J.-P. Ampuero, S. Wei, R. Chu, et al. (2011), The 2011 magnitude 9.0 tohoku-oki earthquake: Mosaicking the megathrust from seconds to centuries, *science*, *332*(6036), 1421–1425.

Singh, S., L. Astiz, and J. Havskov (1981), Seismic gaps and recurrence periods of large earthquakes along the mexican subduction zone: a reexamination, *Bull. Seism. Soc. Am.*, *71*(3), 827–843.

Smith, B., and D. Sandwell (2004), A three-dimensional semianalytic viscoelastic model for time-dependent analyses of the earthquake cycle, *J. Geophys. Res.*, *109*.

Sobolev, S. V., and I. A. Muldashev (2017), Modeling seismic cycles of great megathrust earthquakes across the scales with focus at postseismic phase, *Geochemistry, Geophysics, Geosystems*.

Sone, H., and T. Shimamoto (2009), Frictional resistance of faults during accelerating and decelerating earthquake slip, *Nature Geosci.*, *2*, 705–708.

Suenaga, N., S. Yoshioka, and T. Matsumoto (2016), Relationships among temperature, dehydration of the subducting philippine sea plate, and the occurrence of a megathrust earthquake, low-frequency earthquakes, and a slow slip event in the tokai district, central japan, *Physics of the Earth and Planetary Interiors*, *260*, 44–52.

Suito, H. (2017), Importance of rheological heterogeneity for interpreting viscoelastic relaxation caused by the 2011 tohoku-oki earthquake, *Earth, Planets and Space*, *69*(1), 21.

Sun, T., K. Wang, T. Iinuma, R. Hino, J. He, H. Fujimoto, M. Kido, Y. Osada, S. Miura, Y. Ohta, and Y. Hu (2014), Prevalence of viscoelastic relaxation after the 2011 Tohoku-oki earthquake, *Nature*, *514*, 84–87.

Takeuchi, C. S., and Y. Fialko (2013), On the effects of thermally weakened ductile shear zones on postseismic deformation, *J. Geophys. Res.*, *118*(12), 6295–6310.

Thatcher, W. (1989), Earthquake recurrence and risk assessment in circum-pacific seismic gaps, *Nature*, *341*(6241), 432–434.

Toh, A., K. Obana, and E. Araki (2018), Distribution of very low frequency earthquakes in the nankai accretionary prism influenced by a subducting-ridge, *Earth and Planetary Science Letters*, *482*, 342–356.

Tomita, F., M. Kido, Y. Ohta, T. Iinuma, and R. Hino (2017), Along-trench variation in seafloor displacements after the 2011 tohoku earthquake, *Science advances*, *3*(7), e1700,113.

Toro, G. D., D. L. Goldsby, and T. E. Tullis (2004), Friction falls towards zero in quartz rock as slip velocity approaches seismic rates, *Nature*, *427*, 436–439.

Tsang, L. L. H., E. M. Hill, S. Barbot, Q. Qiu, L. Feng, I. Hermawan, P. Banerjee, and D. H. Natawidjaja (2016), PCAIM models of postseismic deformation with afterslip and viscoelastic deformation following the 2007 Mw 8.6 Bengkulu earthquake, *J. Geophys. Res.*

Tse, S. T., and J. R. Rice (1986), Crustal earthquake instability in relation to the depth variation of frictional slip properties, *J. Geophys. Res.*, *91*(B9), 9452–9472.

Uphoff, C., S. Rettenberger, M. Bader, E. H. Madden, T. Ulrich, S. Wollherr, and A.-A. Gabriel (2017), Extreme scale multi-physics simulations of the tsunamigenic 2004 sumatra megathrust earthquake, in *Proceedings of the International Conference for High Performance Computing, Networking, Storage and Analysis*, p. 21, ACM.

Van Dissen, R. J., and K. R. Berryman (1996), Surface rupture earthquakes over the last 1000 years in the wellington region, new zealand, and implications for ground shaking hazard, *Journal of Geophysical Research: Solid Earth*, *101*(B3), 5999–6019.

Vigny, C., W. Simons, S. Abu, R. Bamphenyu, C. Satirapod, N. Choosakul, C. Subarya, A. Socquet, K. Omar, H. Abidin, et al. (2005), Insight into the 2004 sumatra–andaman earthquake from gps measurements in southeast asia, *Nature*, *436*(7048), 201.

Wada, I., and K. Wang (2009), Common depth of slab-mantle decoupling: Reconciling diversity and uniformity of subduction zones, *Geochemistry, Geophysics, Geosystems*, *10*(10).

Wallace, L., E. Araki, D. Saffer, X. Wang, A. Roesner, A. Kopf, A. Nakanishi, W. Power, R. Kobayashi, C. Kinoshita, et al. (2016), Near-field observations of an offshore mw 6.0 earthquake from an integrated seafloor and subseafloor monitoring network at the nankai trough, southwest japan, *Journal of Geophysical Research: Solid Earth*, *121*(11), 8338–8351.

Wallace, L. M., and J. Beavan (2006), A large slow slip event on the central hikurangi subduction interface beneath the manawatu region, north island, new zealand, *Geophysical Research Letters*, *33*(11).

Wang, K. (2007), Elastic and viscoelastic models of crustal deformation in subduction earthquake cycles, *The seismogenic zone of subduction thrust faults*, pp. 540–575.

Wang, K., and Y. Fialko (2018), Observations and modeling of coseismic and postseismic deformation due to the 2015 mw 7.8 gorkha (nepal) earthquake, *Journal of Geophysical Research: Solid Earth*, *123*(1), 761–779.

Wang, K., Y. Hu, and J. He (2012), Deformation cycles of subduction earthquakes in a viscoelastic earth, *Nature*, *484*(7394), 327.

Wright, T. J., N. Houlié, M. Hildyard, and T. Iwabuchi (2012), Real-time, reliable magnitudes for large earthquakes from 1 hz gps precise point positioning: The 2011 tohoku-oki (japan) earthquake, *Geophysical Research Letters*, *39*(12).

Wu, Y., and X. Chen (2014), The scale-dependent slip pattern for a uniform fault model obeying the rate-and state-dependent friction law, *J. Geophys. Res.*, *119*(6), 4890–4906.

Yabe, S., and S. Ide (2017), Slip-behavior transitions of a heterogeneous linear fault, *J. Geophys. Res.*, *122*(1), 387–410.

Yagi, Y., and Y. Fukahata (2011), Rupture process of the 2011 tohoku-oki earthquake and absolute elastic strain release, *Geophysical Research Letters*, *38*(19).

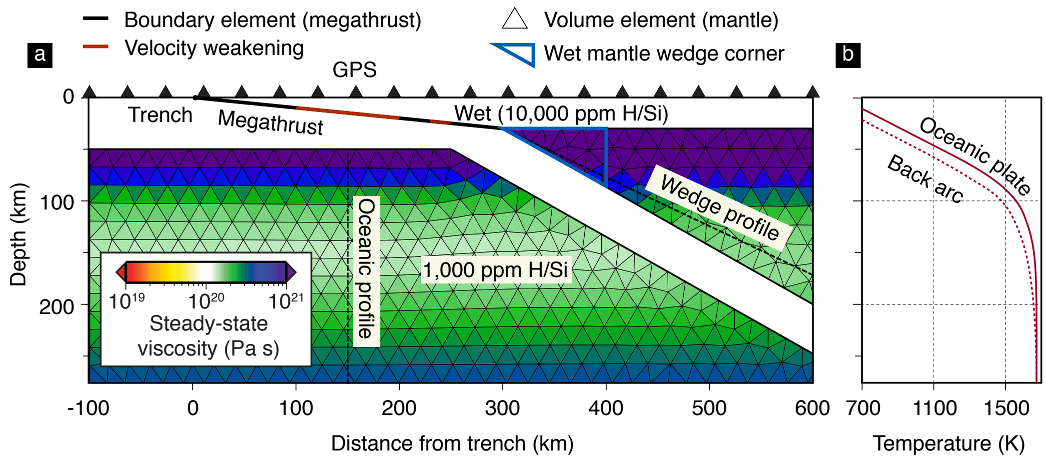

Figure 1. Schematic of a two-dimensional subduction zone model in plane strain with the integral method. a) Geometry of the subduction zone model, mesh elements, and physical properties. Fault slip is represented with boundary elements (segments); plastic strain within the lithosphere is represented with volume elements (triangles with steady-state viscosity). Earthquakes and slow-slip events occur in velocity-weakening fault patches (red line). The mantle wedge corner (blue triangle) is wetter than the surrounding mantle, with $C_{\text{OH}} = 10,000$ ppm H/Si. The region close to the subducting slab interface is elastic and not meshed. The dashed lines indicate the location of the strain-rate and effective viscosity profiles in Figures 2 and 3. The displacement history is evaluated at the surface, simulating the measurements of geodetic stations (GPS, black triangles). The steady-state viscosity corresponds to the combined effect of diffusion and dislocation creep for a constant shortening rate of -10^{-15} /s. b) Vertical temperature profiles assumed in the oceanic plate and the backarc region. The physical properties in the upper mantle are vertically stratified, except for different temperatures and water contents in the oceanic asthenosphere and in the mantle wedge.

Yokota, Y., T. Ishikawa, S.-i. Watanabe, T. Tashiro, and A. Asada (2016), Seafloor geodetic constraints on interplate coupling of the nankai trough megathrust zone, *Nature*, *534*(7607), 374.

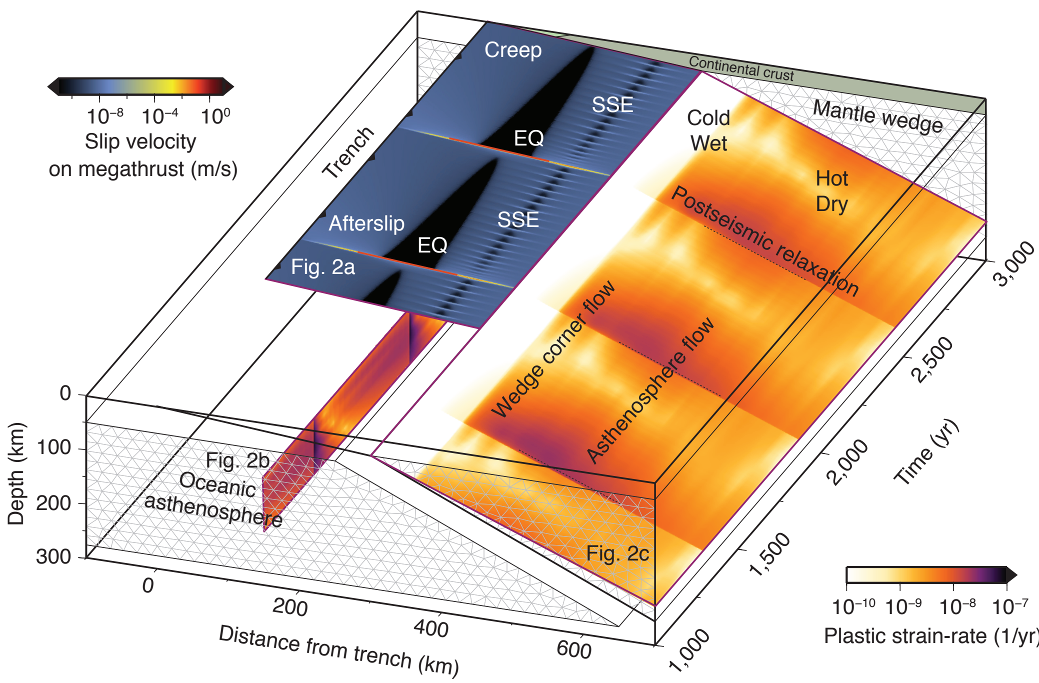

Figure 2. Evolution of the kinematics of fault slip and viscous strain in space and time in a two-dimensional, plane-strain subduction zone model. The x and z-axes indicate the distance from the trench and the depth, respectively. The y-axis indicates the time evolution of the system in cross-section. Earthquakes (EQ) and slow-slip events (SSE) occur on a long megathrust (low-angle fault with colors indexed by the instantaneous slip velocity) cross-cutting the continental crust. Viscoelastic flow (colored by strain rate) in the upper mantle, modeled with triangular elements (grey mesh), is modulated by the seismic cycle, with short postseismic transients in the oceanic asthenosphere and long periods of strain acceleration in the mantle wedge. While wet, little postseismic relaxation occurs in the cold mantle wedge corner (white region abutting the megathrust). A significant fraction of plastic strain is accommodated during the postseismic period in the asthenosphere.

Table 1. Summary of the physical parameters representing fault slip and upper mantle strain constrained from laboratory experiments [*Nakatani*, 2001; *Hirth and Kohlstedt*, 2003]. Friction properties are for a granitic rock. Diffusion and dislocation creep properties are for wet olivine.

Region	Parameter	Symbol	Value	Remark
Megathrust				
	Shear modulus	G	30 GPa	
	Effective confining pressure	$\bar{\sigma}$	100 MPa	
	Static friction coefficient	μ_0	0.6	
	Direct-effect parameter	a	1×10^{-3}	
	Steady-state parameter	$b - a$	-4×10^{-3}	velocity-strengthening
			2×10^{-3}	seismogenic zone
			1×10^{-3}	slow-slip region
	Characteristic weakening distance	L	5 cm	slow-slip region
			50 cm	elsewhere
	Loading rate	V_l	10^{-9} m/s	
	Reference slip velocity	V_0	10^{-6} m/s	
	Shear wave speed	V_s	3×10^3 m/s	
Upper mantle				
	Driving strain rate	$\dot{\epsilon}_{22}^0$	-10^{-15} s^{-1}	all other components 0.
	Basal mantle temperature	1673	K	
Dislocation creep				
	Pre-factor	A_1	90 MPa^{-n} s^{-1} (ppm H/Si)$^{-r_1}$	
	Power-law stress exponent	n	3.5	
	Activation energy	Q_1	480 kJ/mol	
	Activation volume	Ω_1	11×10^{-6} m^3/mol	
	Water fugacity exponent	r_1	1.2	
Diffusion creep				
	Pre-factor	A_2	10^6 MPa^{-1} s^{-1} μm^m (ppm H/Si)$^{-r_2}$	
	Grain size	d	10 mm	
	Grain size exponent	m	3	
	Activation energy	Q_2	335 kJ/mol	
	Activation volume	Ω_2	4×10^{-6} m^3/mol	
	Water fugacity exponent	r_2	1.0	

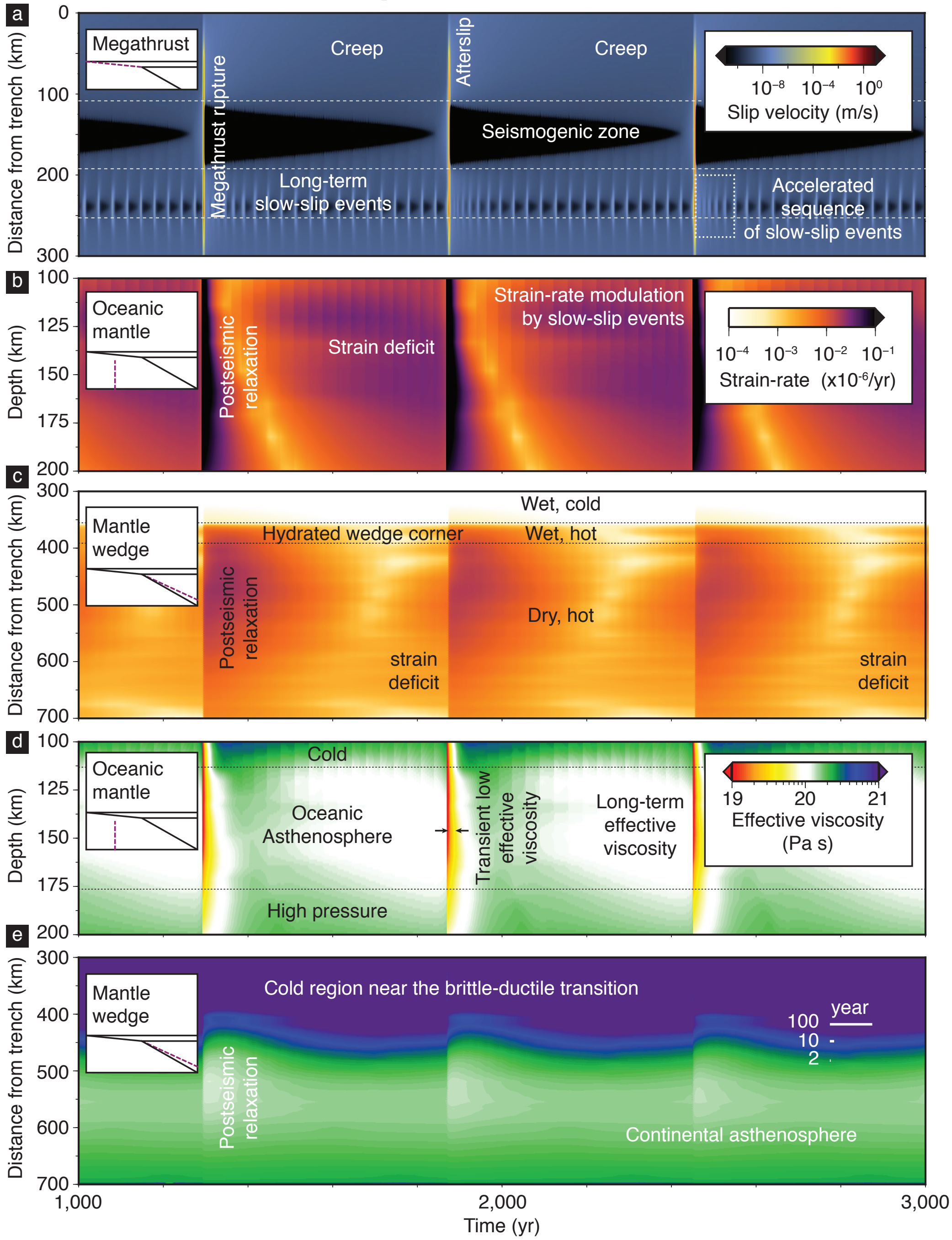

Figure 3. Time series of slip velocity on the megathrust, and strain-rate and effective viscosity in the upper mantle. a) Earthquakes break all of the seismogenic zone every 500 yr and long-term slow-slip events emerge every 25 yr on average. The slow-slip event cycle is accelerated for about one hundred years following fast earthquakes. b) The plastic flow in the oceanic asthenosphere and c) mantle wedge is modulated by the seismic cycle. As the mantle wedge corner extends to cold, shallow depth, little postseismic relaxation occurs there, despite the high water content. d) In the oceanic asthenosphere, the nonlinear dependence to stress of dislocation creep leads to rapid postseismic transients with an effective viscosity reduced by at least an order of magnitude. e) Postseismic viscoelastic flow in the mantle wedge concentrates in a region between 450 and 600 km from the trench, and is little affected by the presence of water below the brittle-ductile transition. The modulation of effective viscosity is less pronounced in the mantle wedge than in the oceanic mantle due to the greater distance between the earthquake rupture and the warm regions of the backarc.

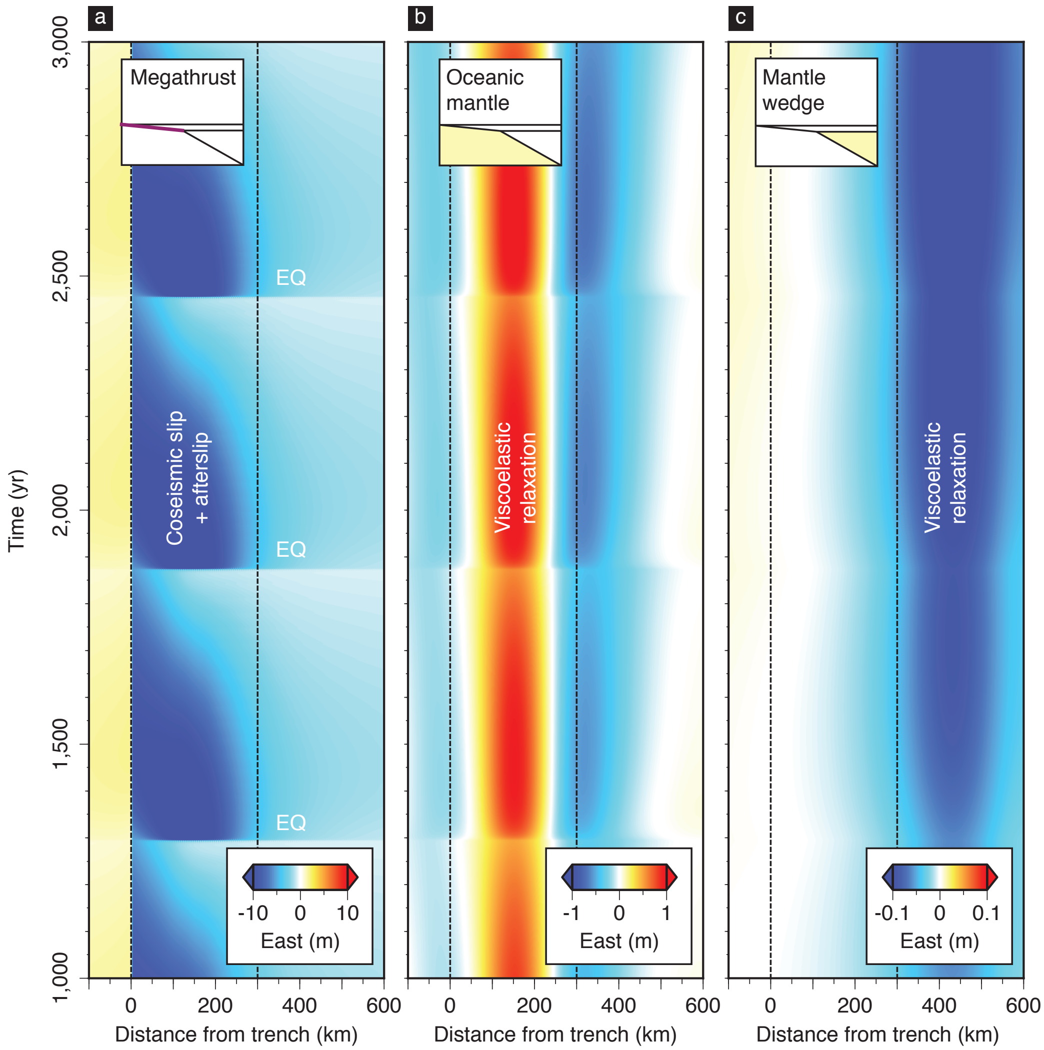

Figure 4. Contribution of (a) fault slip, (b) flow in the oceanic asthenosphere, and (c) flow in the mantle wedge to trench perpendicular surface displacements throughout the seismic cycle. (a) Fault slip produce seaward displacements above the megathrust and small landward displacement in the outer-rise. (b) Postseismic viscoelastic flow in the oceanic asthenosphere produces landward surface displacements above the coseismic rupture and mostly seaward displacements outside this region. (c) Postseismic relaxation in the mantle wedge is weaker under my modeling assumptions, and produces mostly seaward displacement above the land, 300 km and beyond from the trench. Due to the high viscosity in the mantle wedge, the postseismic relaxation following an earthquake still continues when a new one occurs.